ON TRACER SELECTION AND TRACKING IN WV IMAGES

Angeles Hernandez-Carrascal

School of Systems Engineering, University of Reading, Whiteknights, Reading RG6 6AY, U.K.

Abstract

This paper presents recent and ongoing work in the area of tracer selection and tracking in water vapour imagery, in the context of atmospheric motion vector (AMV) derivation. First, it investigates the contribution of different spatial frequencies to the tracking, using MSG-2 water vapour images and following an approach based on Gaussian multi-scale representation; the main finding is that the higher frequencies might have a negative impact on the tracking. It also describes results of a preliminary study concerning tracer selection. Finally it introduces the H_1 norm as a similarity function for the tracking step; H_1 is based on the familiar L_2 norm, but, unlike L_2, it includes terms for the spatial derivatives.

1 INTRODUCTION

An aspect of the derivation of atmospheric motion vectors (AMV) that has received considerable attention lately is tracer selection, and in particular, the impact of tracer size on AMV quality. On the one hand, smaller tracers contain less information, and are more likely to produce low quality AMVs, especially for large time intervals between consecutive images, as shown by Dew and Ackermann (2010). On the other, larger tracers are more likely to contain features from different layers, and therefore to produce winds that actually are averages of winds from different levels, as suggested by Sohn and Borde (2008).

Daniels and Bresky (2010) have proposed a nested tracking method to retain the advantages of both large and small tracers, and have shown that their method diminishes the slow speed bias, a known problem in AMV derivation, especially with the 10.8 μm imagery. Several studies have investigated the relation between optimal tracer size and time interval between images (Oyama, 2010; Cho and Ou, 2010).

Another aspect to consider is the detection of promising tracers: is it possible to characterize good (or bad) tracers, i.e. is it possible to find a meaningful statistical relation between the local properties of tracer boxes and the quality of the resulting AMVs? Not all tracers yield good AMVs, and suitable criteria allowing an a priori selection of promising tracers may contribute to a better overall quality of the motion field and to a better use of the available computing resources. In the IR 10.8 μm imagery, often strong gradients are sought, as they allow the detection of well defined cloud edges. However, the nature of WV imagery is different (e.g. there are no sharp edges); operational derivation schemes (Holmlund, 2002; Velden et al, 1997) typically include a tracer selection step that preferably locates tracers in areas of strong gradients in cold areas of the image.

This paper presents recent and ongoing research in the area of tracer selection and tracking in water vapour imagery. Although the main thread of the work is tracer selection, it has lead to other areas, such as spatial frequencies or similarity functions. The patchwork style perhaps reflects the deep connection between the different aspects of the problem of AMV derivation.

The structure of this paper is as follows. Section 2 briefly introduces the basic framework used throughout the paper, Gaussian multi-scale representation. Section 3 studies the contribution of different frequencies to the tracking, for a number of tracer sizes. Section 4 presents results of preliminary data analysis regarding the relation between local properties of tracers and the quality of the motion field. Section 5 introduces a new similarity function, based on the H_1 norm, and section 6 concludes the paper.

2 GAUSSIAN MULTI-SCALE REPRESENTATION

Gaussian multi-scale representation (Lindeberg, 1994) is a very successful approach in computer vision. An image $I(x, y)$ is embedded in a family of convolutions with the 2-dimensional Gaussian kernel G:

$$L(.,.;\sigma) = G(.,.;\sigma) * I(.,.) \qquad (\sigma \in \mathbb{R}^+) \tag{1}$$

where

$$G(x, y, \sigma) = \frac{1}{2\pi\sigma^2}\, e^{-\frac{x^2+y^2}{2\sigma^2}} \qquad (x, y \in \mathbb{R}) \tag{2}$$

Each $L(x, y; \sigma)$ can be seen as a smoothed version of the original image $I(x, y)$, and the original image I is the member of the family for $\sigma = 0$. In equation (1), semicolon has been used as separator to stress the different roles of σ and the spatial variables.

The Gaussian function is a regularizing kernel with many good properties, extensively discussed in the literature by e.g. Lindeberg (1994), Florack et al. (1992), Marr and Hildreth (1980) and Stein and Shakarchi (2003). In particular, it provides an optimal compromise between space localization and frequency localization (Marr and Hildreth, 1980), and convolution with a Gaussian kernel does not introduce spurious structures (Lindeberg, 1994).

The properties of the Gaussian kernel make Gaussian multi-scale representation a sound and efficient framework to analyze images. It can be used to study the contribution of different frequencies, and it also provides a natural and efficient way of calculating derivatives in a generalized sense. Note that it does not really make sense to talk about the partial derivatives of I in the traditional sense, as it might not even be continuous. But when I is seen as embedded in a family of convolutions with the 2-D Gaussian kernel, as described in equation (1), it is possible to consider the partial derivatives, in a generalized sense:

$$D_x I(.,.;\sigma) = \frac{\partial G}{\partial x}(.,.;\sigma) * I(.,.) \tag{3}$$

and

$$D_y I(.,.;\sigma) = \frac{\partial G}{\partial y}(.,.;\sigma) * I(.,.) \tag{4}$$

A simple calculation gives:

$$\frac{\partial G}{\partial x}(x, y, \sigma) = -\frac{x}{\sigma^2}\, G(x, y, \sigma) \qquad \text{and} \qquad \frac{\partial G}{\partial y}(x, y, \sigma) = -\frac{y}{\sigma^2}\, G(x, y, \sigma) \tag{5}$$

which allows the efficient computation of $D_x I(.,.;\sigma)$ and $D_y I(.,.;\sigma)$. Note that the derivatives of I are necessarily linked to a particular value of σ, i.e. to a scale, and that derivatives for $\sigma = 0$ (i.e. the original image) are not defined.

3 SPATIAL FREQUENCIES

This section studies the contributions of different spatial frequencies to the tracking, using the framework introduced in the previous section. The initial motivation for this study was the need of background knowledge about the effect of Gaussian smoothing on the tracking. As mentioned earlier, tracer selection is the main thread of this work, and the scale at which properties are observed is an important issue. For this reason, knowledge about the role of scale on the tracking was considered necessary. The study focussed on image analysis aspects.

Each Gaussian blur $L(x, y, \sigma)$, result of the convolution of the original image $I(x, y)$ with the 2-dimensional Gaussian kernel, as described in equation (1), is essentially a smoothed version of the original image from which the higher spatial frequencies have been removed, i.e. a Gaussian blur is a low-pass filter. Similarly, the difference between two Gaussian blurs

$$D(x, y; \sigma_1, \sigma_2) = L(x, y; \sigma_1) - L(x, y; \sigma_2) \quad (6)$$

can be seen as the result of removing the higher and lower frequencies from the original image $I(x, y)$, i.e. it is a band-pass filter.

The data used in the experiments were brightness temperatures from the MSG-2 water vapour 6.2 μm channel, with a time interval of 15 minutes between consecutive images. The area (south-western Europe and North Africa) is shown in figure 1 with the help of an IR 10.8 μm image. The date and time of the images is 17 July 2007, between 10 and 11 UTC. Concerning the tracking, the similarity function used was Euclidean distance, and a search area of 30 pixels around tracer boxes was used. The backtracking test was used to evaluate the resulting motion vectors. Note that height assignment is not attempted.

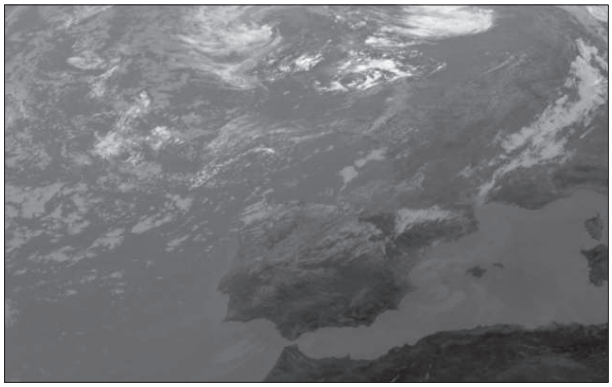

Figure 1: **IR image showing the area used in the test.**

The backtracking test is essentially an inverse consistency test. Assume that we select a tracer box B_1 in an image I_1 and calculate its best match B_2 in the next image I_2, according to a particular method, yielding a vector $\mathbf{v}$. If the method is good for successfully calculating the apparent motion from I_1 to I_2 in the neighbourhood represented by B_1, it will also be good to estimate the apparent motion from I_2 to I_1 in a neighbourhood of B_2, and the new vector will be $-\mathbf{v}$. Let B_{1a} be the best match for B_2 in I_1. The distance between B_1 and B_{1a} can be used to classify the motion vectors (MV): an MV is assigned to class $F0$ if B_{1a} is identical to B_1, to class $F1$ if B_{1a} is not identical to B_1 but it is one pixel apart in x and/or y directions, and to class $F9$ otherwise. An MV is labelled as ”good” if it is either in $F0$ or in $F1$. The backtracking test is a simple consistency test, and a good method to derive MVs should yield a high percentage of ”good” vectors. However, the evidence this test gives is limited, and for a thorough assessment it should be complemented with other evaluation methods, such as comparison with NWP wind fields or radiosonde observations.

To generate the sample, a selection grid with 8 pixels between grid points in both directions was used. The tracer sizes considered were $20 * 20$, $24 * 24$, $28 * 28$, $32 * 32$ and $36 * 36$. Table 1 shows the number of tracers in each sample. Note that this number varies with tracer size; the reason is that for larger sizes less tracers can be selected, for this sampling process. Before starting with the experiments on frequencies, we run the experiment on the original images, in order to get a reference. Figure 2 shows the results; the y-axis represents the percentage of tracers in each of the groups $F0$, $F1$ and $F9$. Displacements $v = 0$ (less than 10%) have not been included, as they are not considered meaningful.

Tracer size (pixels)	20*20	24*24	28*28	32*32	36*36
Number of tracers	3552	3436	3402	3283	3274

Table 1: **Number of tracers in the sample for each tracer size.**

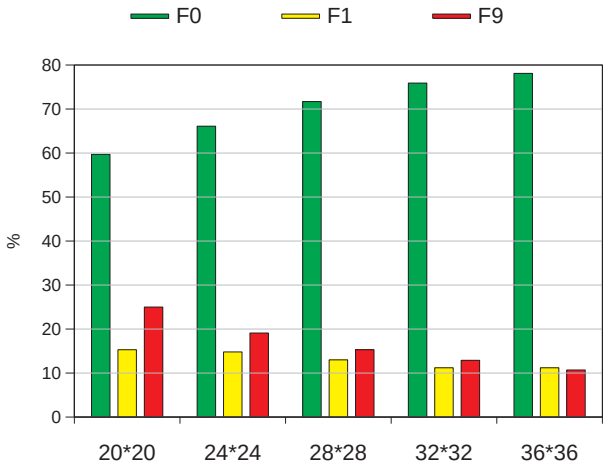

Figure 2: **percentage of tracers in each group, for each tracer size.**

The purpose of the first experiment with frequencies was to investigate the contribution of higher frequencies to the tracking, by using smoothed images, as described in equation (1), instead of the originals, for a number of values of σ. The results are shown in figure 3. The y-axis represents the percentage of tracers in either $F0$ or $F1$. Each line in the plot is associated to a tracer size. A consistent improvement, as tracer size increases, can be seen for every value of σ tested, as one would expect, and in agreement with the results shown earlier in figure 2. Note that the values for $\sigma = 0$ are the same as those in figure 2, as both correspond to the original images.

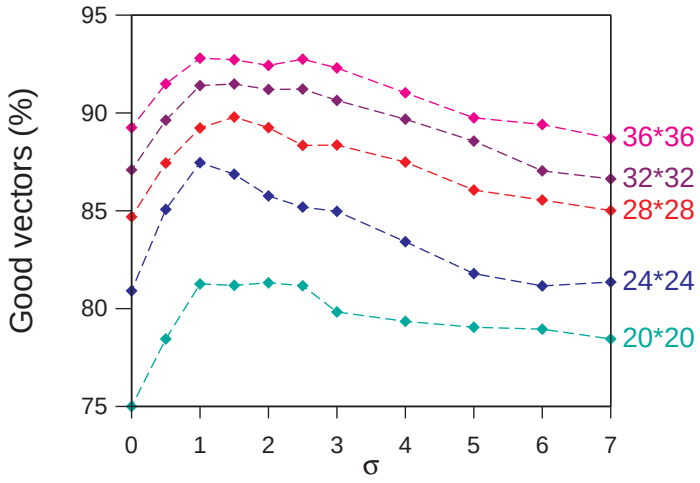

Figure 3: **relation between percentage of good vectors and σ for several tracer sizes.**

More surprising is the shape of the lines relating the percentage of good MVs to σ. In all cases, this percentage increases sharply from $\sigma = 0$ (i.e. the original set) to $\sigma = 1$, peaks in the interval $[1, 2]$ and then decreases. This pattern is consistently observed for all the tracer sizes tested, and suggests that the higher spatial frequencies actually have a negative impact on the tracking. It is not clear whether this might happen because higher frequencies contain higher levels of noise, or because they are associated to small-scale non-advective atmospheric disturbances. Further research could study their relative contributions.

In the second experiment with frequencies, differences between Gaussian blurs, as described in equation (6), were used. The differences between Gaussian blurs are band-pass filters, and the values of σ_1 and σ_2 determine the range of frequencies retained. By keeping constant σ_1 and varying σ_2 it is possible to study the contribution of lower frequencies to the tracking. Figure 4 shows the results of this experiment. Each panel contains two lines, one for $\sigma_1 = 0$ (i.e. original images, without smoothing), and another for $\sigma_1 = 1$. The six curves show an improvement as σ_2 increases, suggesting that lower frequencies have a positive impact for the range considered; however, this improvement soon becomes marginal. Results for $\sigma_1 = 1$ are consistently better than for $\sigma_1 = 0$, in agreement with the results shown earlier in figure 3.

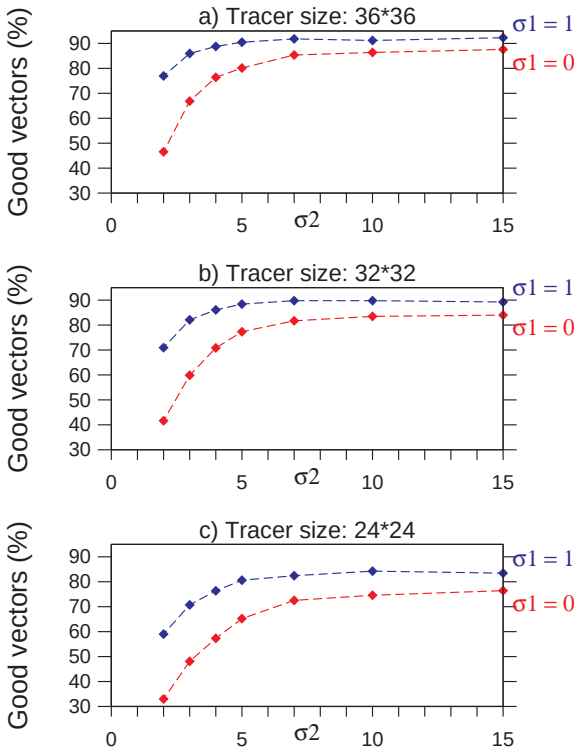

Figure 4: **See text.**

4 TRACER PROPERTIES

This section briefly describes the results of a preliminary study carried out with the aim of exploring the relationship between the local properties of tracers and the quality of the MVs produced. Two main issues arise when approaching this problem: 1) what tracer properties should be analyzed, and 2) at what scale.

With the setup described in section 3, histograms and scatter plots were generated for a number of values of σ, between 0 and 6. Several variables that reflect local variation (standard deviation, contrast, gradient) were analysed, and local maximum and minimum brightness temperatures were also included. The image sequence corresponding to $\sigma = 1$ was used for tracking, as this was the value that consistently produced the best results for all tracer sizes in the experiment described in the previous section.

Figure 5 shows two such histograms, both for $\sigma = 1$. Each green, yellow and red bar shows the percentage of tracers labelled as F0, F1 and F9, respectively, in that particular bin. The grey bar shows the number of tracers in the bin. If we concentrate on the region where the number of vectors is significant, the proportion of good vectors shows a slight improvement with stronger gradients, perhaps more noticeable for the $24 * 24$ tracers. On the whole, figures for other values of σ, other tracer sizes

and other variables such as local standard deviation or local contrast showed similar results. However, scatter plots for minimum *BT* and maximum *BT* for large values of σ showed a strong signal (see figure 6), locating ”bad” tracers preferably in a well defined small area. Further exploration showed a clear concentration of *F*9 tracers on a specific area of the satellite image (not shown) suggesting that the quality of the MV field was linked to large-scale atmospheric flow characteristics more strongly than to local characteristics of the image.

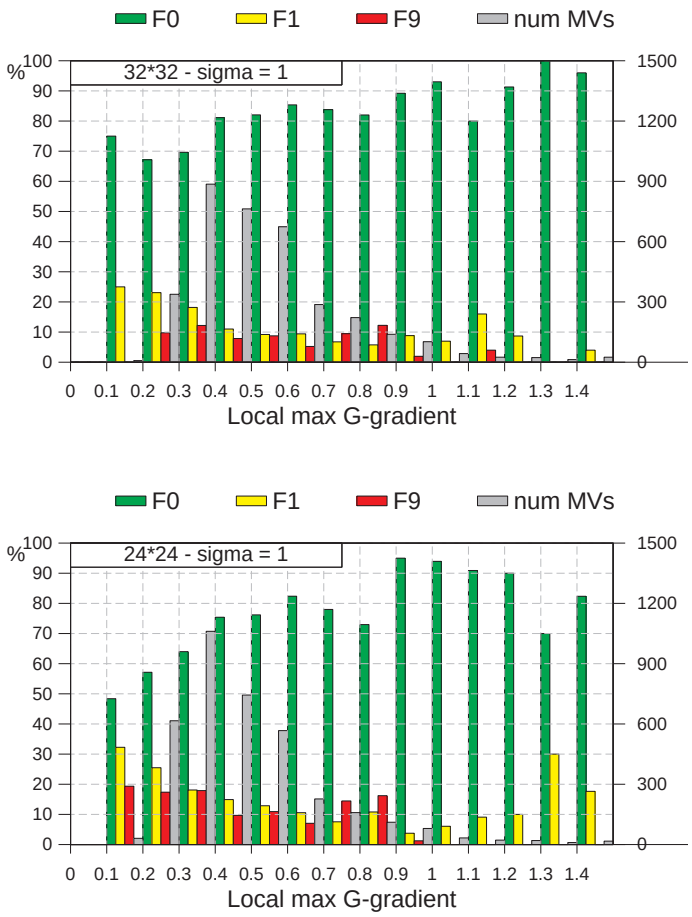

Figure 5: **Histograms showing the distribution of F0, F1 and F9 tracers.**

5 THE H1 NORM AS SIMILARITY FUNCTION

This section introduces the norm H_1 as a similarity function for the tracking step. Sobolev spaces are sometimes used to model images (Chan and Shen, 2005) and in particular the Sobolev space H_1 is often used in image processing. The H_1 norm takes into account not only the values of the function that defines the image (such as brightness temperature or radiances) but also its partial derivatives. The motivation to explore this norm is its potential to extract information from tracers, thanks to the terms including derivatives, which might have a positive impact on the quality of MVs, and perhaps allow smaller tracers to be used.

Euclidean distance is often used to measure the similarity of two images. If *I* is an image, the Euclidean norm

$$\|I\|_2 = \{ \sum_{j=j_1}^{j_n} \sum_{i=i_1}^{i_n} I(i,j)^2 \}^{\frac{1}{2}} \tag{7}$$

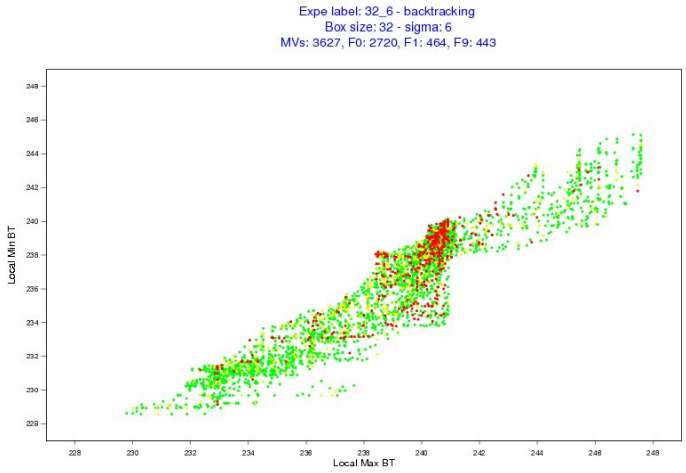

Figure 6: **See text in section 4**

can be seen as the discretization of the L_2 norm:

$$\|I\|_2 = \{\int_\Omega |I(x)|^2\, dx)\}^{\frac{1}{2}} \tag{8}$$

The Sobolev space $H_1(\Omega)$ is a function space related with $L_2(\Omega)$. Unlike the L_2 norm, the H_1 norm includes terms for the partial derivatives $\partial I/\partial x$ and $\partial I/\partial y$:

$$\|I\|_{H_1} = \{\|I\|_2^2 + \|\frac{\partial I}{\partial x}\|_2^2 + \|\frac{\partial I}{\partial y}\|_2^2\}^{\frac{1}{2}} \tag{9}$$

In practice, discretization leads to the expression:

$$\|I\|_{H_1} = \{\sum_{j=j_1}^{j_n}\sum_{i=i_1}^{i_n} I(i,j)^2 + \sum_{j=j_1}^{j_n}\sum_{i=i_1}^{i_n} D_x I(i,j)^2 + \sum_{j=j_1}^{j_n}\sum_{i=i_1}^{i_n} D_y I(i,j)^2\}^{\frac{1}{2}} \tag{10}$$

As mentioned in section 2, it does not make sense to talk about derivatives of I in the traditional sense. However, when I is seen as embedded in a family of Gaussian blurs, the partial derivatives are understood in a generalized sense, and there is a natural and efficient way of calculating the derivatives of I as convolutions of the original image with the derivatives of the Gaussian filter, as described in section 2.

It is also possible to consider an alternative similarity function where different weights are given to the terms in equation (10). First exploratory tests (not shown) suggest that this may be a useful approach. However, it is computationally very costly, which could be a serious drawback.

6 CONCLUSION

This paper has presented recent and ongoing research related to tracer selection and tracking in water vapour imagery, in the context of AMV derivation. It has described a study on the contribution of different spatial frequencies to the tracking, for a range of tracer sizes. The main finding is that the higher frequencies might actually have a negative impact on the tracking; this is a consistent result for all the tracer sizes considered. The contribution of lower frequencies seems to be positive or neutral.

This study should be extended to larger areas and periods, using evaluation methods such as comparison with NWP short-range forecasts and with radiosonde observations. Plans for future work include these extensions. Similar experiments could be carried out with images from other SEVIRI spectral

bands or other satellites, and further research could help understand the reasons for the observed negative impact of the higher frequencies.

The exploratory data analysis regarding the relationship between local properties of the image and the quality of the resulting MVs suggests that there might be a stronger relationship between the overall quality and the large-scale characteristics of the atmospheric flow than with the local properties of the image. However, the study is in early stages.

The paper has also presented the background and motivation for exploring the H_1 norm as a similarity function in tracking. Plans for the future include experimentation with H_1.

REFERENCES

Buche, G., H. Karbstein, A. Kummer, and H. Fischer (2006). Water Vapor Structure Displacements from Cloud-Free Meteosat Scenes and Their Interpretation for the Wind Field. Journal of Applied Meteorology and Climatology, **45**, 4, pp 556–575.

Chan, T. F. and J. Shen (2005). Image Processing and Analysis: Variational, PDE, Wavelet, and Stochastic Methods. Society for Industrial and Applied Mathematics, Philadelphia, USA.

Cho, H., and M. Ou (2010). Determining optimal conditions for mesoscale AMVs. Proc. 10th Int. Winds Workshop, Tokyo, Japan, 22-26 Feb 2010.

Daniels, J. and W. Bresky (2010). A nested tracking approach for reducing the slow speed bias associated with atmospheric motion vectors (AMVs). Proc. 10th Int. Winds Workshop, Tokyo, Japan, 22-26 Feb 2010.

Dew, G., and J. Ackermann (2010). AVHRR polar winds derivation at EUMETSAT: current status and future developments. Proc. 10th Int. Winds Workshop, Tokyo, Japan, 22-26 Feb 2010.

Florack, L. M. J, B. M. ter Haar Romeny, J. J Koenderink, and M. A. Viergever (1992). Scale and the Differential Structure of Images. Image and Vision Computing, **10**, 6, pp 376–388.

Holmlund, K. (2002). Current Status of the EUMETSAT Operational and Future AMV Extraction Facilities. Proc. 6th Int. Winds Workshop, Madison, Wisconsin, USA, 7-10 May 2002.

Lindeberg, T. (1994). Scale-space Theory: A Basic Tool for Analysing Structures at Different Scales. Journal of Applied Statistics, **21**, 2, pp 225–270.

Marr, D., and E. Hildreth (1980). Theory of Edge Detection. Proc. R. Soc. London B **207**, pp 187-217.

Oyama, R. (2010). Recent upgrades of and activities for atmospheric motion vectors at JMA/MSC. Proc. 10th Int. Winds Workshop, Tokyo, Japan, 22-26 Feb 2010.

Sohn, E. H., and R. Borde (2008). The impact of window size on AMV. Proc. 9th Int. Winds Workshop, Annapolis, Maryland, USA, 14-18 April 2008.

Stein, E. M. and R. Shakarchi (2003). Fourier Analysis: An Introduction. Princeton Lectures in Analysis, Princeton University Press, Oxford, UK.

Velden, C. S., C. M. Hayden, S. J. Nieman, W. P. Menzel, S. Wanzong, and J. S. Goerss (1997). Upper-Tropospheric Winds Derived from Geostationary Satellite Water Vapor Observations. Bulletin of the American Meteorological Society, **78**, 2, pp 173–195.